Nov 5th, 12:00 AM - 12:00 AM

Cold-Formed Steel Lipped Channel Columns Undergoing Local-Distortional-Global Interaction: Experimental and Numerical Investigation

Eliane S. Santos

Pedro Borges Dinis

Eduardo M. Batista

Dinar Camotim

Twenty-Second International Specialty Conference on Cold-Formed Steel Structures
St. Louis, Missouri, USA, November 5 & 6, 2014

Cold-Formed Steel Lipped Channel Columns Undergoing Local-Distortional-Global Interaction: Experimental and Numerical Investigation

Eliane S. Santos[1], Pedro B. Dinis[2], Eduardo M. Batista[1] and Dinar Camotim[2]

Abstract

Experimental and numerical results concerning the post-buckling behavior and strength of fixed-ended cold-formed steel lipped channel columns experiencing interaction involving local, distortional and global buckling (*i.e.*, stemming from the closeness between the critical buckling stresses associated with these three buckling mode types), are reported. After briefly addressing the column specimen geometry selection, the paper presents and discusses the results of an experimental investigation carried out at COPPE, Federal University of Rio de Janeiro (UFRJ, Brazil) and involving *16* columns – its output consists of steel material properties, initial imperfection measurements, equilibrium paths and failure loads/modes. Then, some test results are compared with the values yielded by the corresponding ABAQUS shell finite element simulations. Finally, the paper closes with a brief account of the considerations prompted by the available experimental and numerical ultimate load values, concerning the Direct Strength Method (DSM) design of columns affected by triple (local-distortional-global) mode interaction.

[1] Civil Engineering Program, COPPE, Federal University of Rio de Janeiro, Brazil.
[2] DECivil, ICIST, Instituto Superior Técnico, Universidade de Lisboa, Av. Rovisco Pais, 1049-001 Lisboa, Portugal.

Introduction

Thin-walled cold-formed steel lipped channel columns are prone to local (L), distortional (D) and global (G) buckling – see Figures 1(a)-(d). Depending on the column geometry and end support conditions, its post-buckling behavior and strength may be significantly eroded by interaction phenomena involving these three buckling mode types. Out of them, L-G interaction is already well understood (*e.g.*, the use of the "plate effective width" concept). In the last decade, considerable research has been devoted to L-D interaction, including experimental investigations, numerical simulations and design proposals based on the Direct Strength Method (DSM). Concerning interactions involving distortional and global buckling, namely distortional-global (D-G) and local-distortional-global (L-D-G) interaction, the available literature is much scarcer. In the first case, there are a few recent studies (Rossi *et al*. 2012, Dinis & Camotim 2011, Camotim & Dinis 2013, Dubina *et al.* 2013), but a suitable design approach is still missing. In the second case, research work has been reported by Dinis *et al.* (2011,2012,2014), Santos *et al.* (2012) and Young *et al.* (2013), but only incipient design considerations are available up to now. An interesting preliminary conclusion was the minor role played by the local deformations, which amounts to arguing that the D-G and L-D-G interaction effects are qualitatively and quantitatively similar.

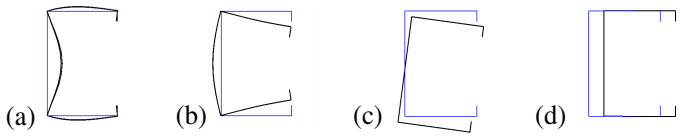

Fig. 1: Lipped channel column cross-section buckled in (a) local, (b) distortional, (c) flexural-torsional and (d) flexural modes

The paper reports numerical and experimental results on the post-buckling and ultimate strength behavior of three sets of fixed-ended cold-formed steel lipped channel columns (in each set, the columns exhibit identical cross-section dimensions and different lengths) experiencing different levels of local-distortional-global interaction. The experimental results, obtained at COPPE (Federal University of Rio de Janeiro) and recently reported by Santos *et al.* (2014), include initial imperfection measurements (displacement profiles), equilibrium paths, collapse modes and failure loads. The numerical results,

provided by ABAQUS shell finite element analyses, consist of equilibrium paths, ultimate strengths and failure mode representations. Moreover, the numerical and experimental ultimate strength data reported, as well as those available in the literature, are also used to discuss possible DSM-based design approaches for lipped channel columns experiencing L-D-G interaction.

Buckling Behavior – Column Geometry Selection

In order to obtain lipped channel column geometries (web width b_w, flange width b_f, stiffener width b_s, wall thickness t and length L) ensuring nearly coincident local, distortional and global critical buckling loads ($P_{crL} \approx P_{crD} \approx P_{crG}$), it was necessary to perform sequences of "educated" trial-and-error buckling analyses using the code GBTUL (Bebiano *et al.* 2008), based on Generalized Beam Theory (GBT), and taking into account that the lipped channel specimens would be manufactured from a structural steel sheet with nominal thickness equal to *1.10 mm*. The end product of the above trial-and-error procedure is illustrated in Figure 2, which shows the ABAQUS shell finite element (SFE) buckling results for columns exhibiting cross-section dimensions b_w=*75 mm*, b_f=*65 mm*, b_s=*11 mm* and t=*1.10 mm* (Dinis *et al.* 2011). The observation of the curve depicted in Figure 2(a), which provides the variation of the critical buckling load P_{cr} with the length L (logarithmic scale), clearly shows that a column with length $L_{L/D/G}$=*2350 mm* has four nearly coincident L, D and G critical loads: $P_{cr.D4}$=*55.9 kN* (*4* distortional half-waves), $P_{cr.D5}$=*56.8 kN* (*5* distortional half-waves), $P_{cr.G}$=*57.1 kN* (single flexural-torsional half-wave) and $P_{cr.L}$=*57.4 kN* (*33* web-triggered local half-waves)[3] – the corresponding buckling mode shapes are depicted in Figure 2(b). This means that the post-buckling behavior and ultimate strength of this column are bound to be highly affected by L-D-G interaction.

The above procedure led to the identification of the three column specimen geometries given in Table 1, together with the corresponding P_{crL}, P_{crD} and P_{crG} values, calculated for E=*210 GPa* and ν=*0.3* (Dinis *et al.* 2011) – note that the critical load values are never more than *3%* apart. In order to analyze columns with different levels of L-D-G interaction effects, it was decided to select three sets of columns with (i) LC1-LC3 cross-section geometries and (ii) lengths

[3] In fixed-ended lipped channel columns, distortional buckling loads associated with buckling modes exhibiting consecutive half-wave numbers are often very close.

that are lower, equal or higher than $L_{L/D/G}$, *i.e.*, exhibiting $P_{crG}>P_{crL}\approx P_{crD}$, $P_{crL}\approx P_{crD}\approx P_{crG}$ or $P_{crG}<P_{crL}\approx P_{crD}$, respectively (Santos *et al.* 2014) – the columns selected have the following geometries: (i) LC1 cross-section and *L=2150*;*2200*;*2350* (=$L_{L/D/G}$); *2500*; *2550*; *2600mm*, (ii) LC2 cross-section and *L=2100* (=$L_{L/D/G}$); *2250*; *2300*; *2350 mm*, and (iii) LC3 cross-section and *L=1500*;*1550*;*1650* (=$L_{L/D/G}$); *1800*;*1850*;*1900mm.*

Table 1: Column specimen geometries and critical local, distortional and global buckling loads

Column specimens	b_w (mm)	b_f (mm)	b_s (mm)	T (mm)	L (mm)	$P_{cr.L}$ (kN)	$P_{cr.D}$ (kN)	$P_{cr.G}$ (kN)	$\frac{P_{cr.max}}{P_{cr.min}}$
LC1	75	65	11	1.10	2350	48.8	47.5	48.6	1.03
LC2	71	60	11	1.10	2100	51.9	51.8	51.9	1.00
LC3	62	55	11	1.10	1650	60.1	58.8	59.5	1.02

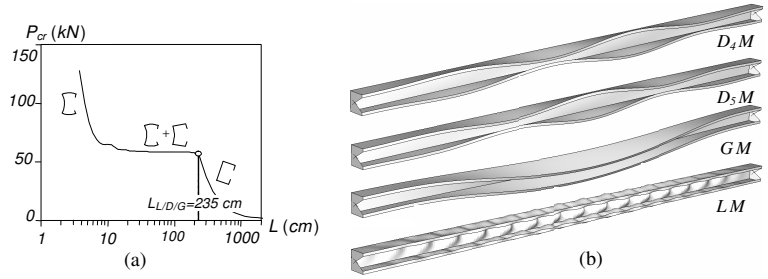

Fig. 2: (a) P_{cr} vs. L curve for columns with b_w=*75 mm*, b_f=*65 mm*, b_s=*11 mm* and t=*1.10 mm*, and (b) $L_{L/D/G}$=*2350 mm* column critical local, distortional and global (flexural-torsional) buckling mode shapes

Experimental Investigation

This section addresses the experimental investigation carried out at COPPE (Federal University of Rio de Janeiro), which was very recently reported by Santos *et al.* (2014). The cold-formed steel lipped channel column specimens were obtained from a structural steel sheets with nominal thickness *1.10 mm* and yield stress f_y=*345 MPa*. The mechanical properties of the structural steel were experimentally measured/quantified by means of standard tensile coupon tests (the coupons were directly extracted from the virgin steel sheets prior to

the initiation of the cold-forming procedure) – the average values of the Young's modulus, yield and failure stresses were E_0=*211 GPa*, f_y=*342 MPa* and f_u=*439MPa* (it was assumed that ν=*0.3* for all steel sheets).

All the measured specimen cross-section dimensions and lengths are given in Table 2, together with the associated P_{crL}, P_{crD} and P_{crG} values (calculated for *E=210 GP*a and ν=*0.3*), and the maximum-to-minimum ($P_{cr.max}/P_{cr.min}$) and intermediate-to-minimum ($P_{cr.int}/P_{cr.min}$) critical load ratios. The *16* specimens were labelled CP2-CP32 (only even numbers were considered) and, in order to check the test repeatability, two nearly identical CP32 specimens were tested. It is worth noting that (i) P_{crL} is always the critical buckling load, because in the actual/measured specimen web widths b_w were found to be consistently higher than the values appearing in Table 1, (ii) the intermediate buckling load is global for *8* columns and distortional for *6* columns (*2* columns have practical identical distortional and global buckling loads), (iii) the P_{crD}/P_{crL} values are in

Table 2: Column specimen (i) geometries, (ii) squash and critical (local, distortional, global) buckling loads, (iii) test failure loads, (iv) observed failure mode nature

Column specimens	b_w (mm)	b_f (mm)	b_s (mm)	t (mm)	L (mm)	P_y (kN)	$P_{cr.L}$ (kN)	$P_{cr.D}$ (kN)	$P_{cr.G}$ (kN)	$\frac{P_{cr.int}}{P_{cr.min}}$	$\frac{P_{cr.max}}{P_{cr.min}}$	$\frac{P_y}{P_{cr.max}}$	P_{Exp} (kN)	Failure mode
CP2	79.4	66.1	11.8	1.08	2600	87.6	44.0	48.1	46.2	1.05	1.09	1.82	38.3	DG
CP4	79.3	66.0	11.8	1.08	2550	87.5	44.0	48.3	47.6	1.08	1.10	1.81	37.3	DG
CP6	78.9	66.0	11.8	1.09	2500	88.2	45.5	49.3	49.3	1.08	1.08	1.79	41.6	DG
CP8	79.6	65.8	12.0	1.09	2350	88.4	45.1	50.7	55.5	1.12	1.23	1.59	36.1	DG
CP10	78.4	66.5	11.9	1.09	2200	88.4	45.9	50.7	59.3	1.11	1.29	1.49	39.8	DG
CP12	79.8	65.7	11.8	1.10	2150	89.1	46.2	51.9	63.3	1.13	1.37	1.41	44.3	DG
CP14	75.3	61.5	11.7	1.09	2350	83.4	47.8	52.5	49.2	1.03	1.10	1.59	34.7	DG
CP16	74.7	61.0	11.9	1.09	2300	82.9	48.4	53.9	50.5	1.04	1.11	1.54	34.8	DG
CP18	75.3	61.1	11.8	1.07	2250	81.6	45.3	51.5	51.7	1.14	1.14	1.58	39.3	DG
CP20	75.2	61.3	11.8	1.08	2100	82.5	46.6	53.3	57.6	1.14	1.24	1.43	37.9	DG
CP22	66.8	56.2	11.8	1.08	1900	75.6	53.3	58.8	55.3	1.04	1.10	1.28	39.5	DG
CP24	66.7	56.0	11.7	1.07	1850	74.6	51.9	57.6	56.6	1.09	1.11	1.30	38.2	DG
CP26	66.6	56.0	11.8	1.07	1800	74.6	52.1	58.0	59.1	1.12	1.14	1.26	35.9	DG
CP28	66.8	55.9	11.8	1.08	1650	75.3	53.3	59.7	67.9	1.12	1.27	1.11	40.2	DG
CP30	66.8	56.0	11.7	1.09	1550	76.0	54.8	61.1	73.6	1.12	1.34	1.03	42.4	DG
CP32	66.5	56.1	11.7	1.08	1500	75.3	53.6	60.7	74.6	1.13	1.39	1.01	43.0	DG
CP32-1	66.6	56.1	11.8	1.06	1500	74.0	50.6	59.2	73.0	1.17	1.44	1.01	43.1	DG

the *1.08-1.14* range, (iv) the P_{crG}/P_{crL} values in the *1.03-1.44* range (only *8* out of *17* values are more than *20%* apart, with only *4* exceeding *30%*), and (v) all the $P_{cr.int}/P_{cr.min}$ values are below *1.18* – these combinations of buckling load ratios make it logical to anticipate that the ultimate strength of all the tested column specimens is likely to be eroded by the triple L-D-G interaction effects.

All specimens were compressed under fixed-ended support conditions, with *12 mm* thick steel plates previously TIG welded to their end sections and then put in contact with (or bolted to) the testing frame loading plates – Figure 3(a) provides a detailed view of the specimen bottom end support. This is done after performing a sequence of operations involving the accurate identification of the locations of the end section centroids, in order to align them with the testing frame axis. This procedure, based on the actual profile of each end section, aims at accurately positioning the column axis, with respect to the testing frame axis, thus minimizing the occurrence of loading eccentricities.

The compressive load is applied (in quasi-static conditions) by means of a servo-controlled displacement system and the experimental data was recorded in a digital acquisition system (with a *15Hz* or higher frequency). The column initial geometrical imperfections and displacement evolution, as loading progresses, are measured through a set of displacement transducers (T) located along the cross-section, as indicated in Figure 3(b). When measuring the initial geometrical imperfections (after applying a small pre-load ≈*1 kN*), all the transducers could be moved along the column length – see Figure 3(c). Once a test started, (i) transducers T1, T3-T5 remained permanently located at the column mid-height cross-section, and (ii) transducers T2, T6 and T7 could be moved along the column length at specific load values (*i.e.*, with the loading process interrupted), making it possible to obtain the corresponding column deformed configuration. While transducers T6 and T7 were able to trace the distortional and global (flexural-torsional) deformations, transducer T2 could detect the local and distortional ones (Fig. 3(d) concerns specimen CP2 and shows the variation of d_6 along the bottom flange-lip longitudinal edge).

The experimental ultimate loads (P_{Exp}) are given in Table 2, which provides also the column failure mode nature – note that the failure loads of specimens CP32 and CP32-1 are practically identical, thus ensuring repeatability. All specimens failed in distortional-global (flexural-torsional) interactive modes (no local deformations were observed or measured) – Figures 4(a_1)-(a_3) show the deformed configurations near collapse of specimens CP2, CP18 and CP28,

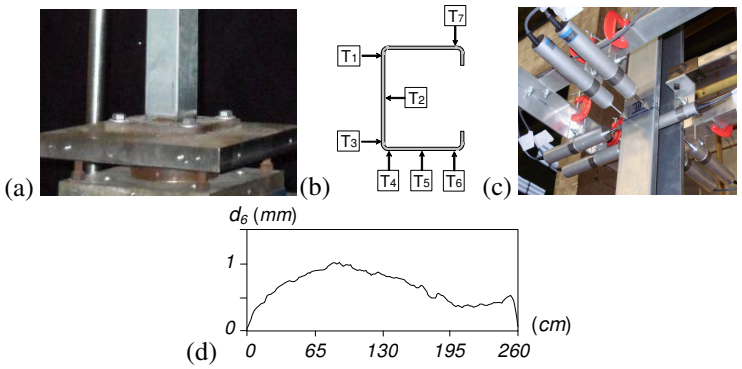

Fig. 3: (a) Specimen bottom end support, (b) location of the displacement transducers, (c) moving device to obtain longitudinal displacement profiles and (d) d_6 displacement longitudinal profile along the bottom flange-lip longitudinal edge (specimen CP2)

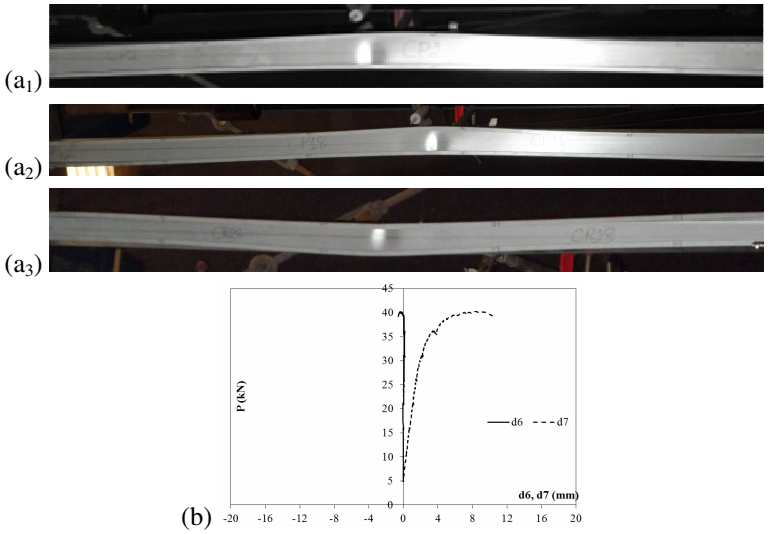

Fig. 4: (a) Experimental evidence of distortional-global interaction in specimens (a_1) CP2, (a_2) CP18 and (a_3) CP28, and (b) specimen CP28 *P vs.* d_6 and *P vs.* d_7 equilibrium paths

clearly evidencing the simultaneous occurrence of distortional and global (flexural-torsional) deformations. As for Figure 4(b), it depicts the *P vs.* d_6 and *P vs.* d_7 equilibrium paths of specimen CP28 – several other equilibrium paths, corresponding to other specimens and/or transducer measurements, were recorded and some of them were recently reported by Santos *et al*. (2014).

Although the observation of this set of experimental column non-linear equilibrium paths and failure modes shows that they are in line with those reported earlier by Santos *et al.* (2012), they still remain rather surprising. This is because they indicate that local deformation play virtually no role in the column response, even when its critical buckling mode is local – moreover, no trace of local deformations was detected during the experimental tests. In order to back this assertion, note that (i) all the specimens tested (CP2-CP32) exhibit local critical buckling stresses and, in several of them, (ii) the P_{crG}/P_{crL} values are not so small (in *8* out of the *17* columns tested this ratio falls in the *1.23-1.44* range) and, at the same time, the P_y values are not significantly above $P_{cr.max}$, *i.e.*, the highest of the local, distortional and global critical buckling loads (the $P_y/P_{cr.max}$ ratio falls inside the *1.01-1.82* range – note that the shorter specimens, CP30 and CP32, exhibit $P_y/P_{cr.max}\approx 1.0$). Two possible explanations for this quite unexpected behavior (absence of local deformations), which did not occur in similar tests recently reported by Young *et al.* (2013), are: either (i) very high global initial imperfection amplitudes or (ii) a test set-up that did not ensure adequate fixed-ended support conditions. The latter is more plausible, since the possibility of (restrained) end section flexural rotations would certainly lead to a (more or less considerable) P_{crG} decrease, which is consistent with the observed occurrence of predominantly global collapses at failure loads lower than expected and, due to the very low global post-critical strength reserve, never involving local deformations.

Numerical Simulations

This section deals with the numerical simulation of the experimental results by means of ABAQUS SFEA that (i) adopt column discretisations into fine 4-node isoparametric element meshes (length-to-width ratio close to *1*), and (ii) model the column supports by attaching rigid plates to their end section centroids. Only a few numerical results, concerning the non-linear behavior and ultimate strength of specimen CP30 (b_w=66.8 *mm*, b_f=56.0 *mm*, b_l=11.7 *mm*, *t*=1.09 *mm* and *L*=1550 *mm* – the shorter specimen tested) are presented,

discussed and compared with the corresponding experimental results. It must be made clear that the following assumptions were adopted to perform the (preliminary– several refinements are planned for the near future) numerical simulation reported herein:

(i) The steel is deemed homogeneous and isotropic, with an elastic-plastic behavior described by a multi-linear model that (i_1) assumes $E=211\ GPa$, $\nu=0.3$ and $f_y=342\ MPa$ (coupon test average values) and (i_2) approximates the measured stress-strain curve, prior to the yield plateau, by linear segments connecting the experimental curve points concerning four stress values ($\sigma=0.72f_y$, $0.87f_y$, $0.95f_y$, f_y) – Figure 5(a) shows a comparison between the experimental stress-strain curve and the multi-linear one adopted to model it in the numerical simulations.

(ii) The column end sections are fixed: with the sole exception of the rigid-body longitudinal displacement of the loaded end section, which is free, all the displacements and rotations are fully prevented.

(iii) Both the residual stresses (not measured in the tested specimens) and corner strength effects are neglected.

(iv) In order to assess the sensitivity of the numerical results to the initial geometrical imperfection shape, various combinations of the (iv_1) local critical buckling mode with twenty five half-waves and amplitude δ_0, (iv_2) distortional critical buckling mode with three half-waves and amplitude Δ_0, and (iv_3) flexural-torsional critical buckling mode with a single half-wave and amplitude β_0 were considered. The Δ_0, δ_0, and β_0 values adopted were obtained by means of the expressions displayed in Figure 5(b), which involve the (iv_1) the d_1-d_7 measured initial displacements and (iv_2) $v_{G.0}$ and $w_{D.0}$ values, which are taken from the cross-section deformed shapes corresponding to the global and distortional critical buckling modes (see Fig. 5(b)). Moreover, these amplitude values, which read $\Delta_0=-0.71\ mm$ $\delta_0=1.05\ mm$ and $\beta_0=0.02\ rad$, were determined on the basis of the higher displacement values measured along the specimen length.

(v) The initial imperfection shapes considered in this study were the following: pure local (IP1), pure distortional (IP2), pure flexural-torsional (IP3), local-distortional (IP4), local-flexural-torsional (IP5), distortional-flexural-torsional (IP6) and local-distortional-flexural-torsional (IP7) initial geometrical imperfections.

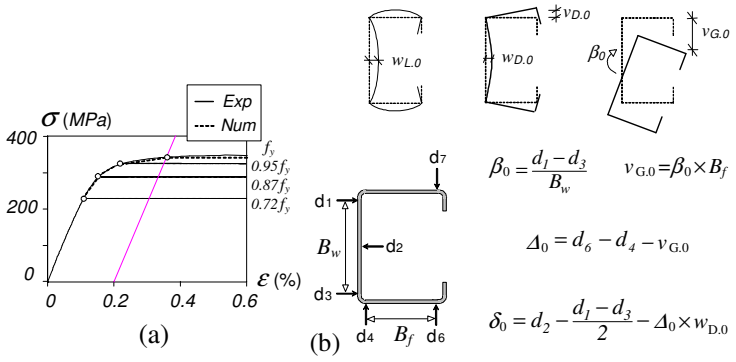

Fig. 5: (a) Comparison between the experimentally obtained and numerically modeled stress-strain curves and (b) amplitudes of critical-mode initial geometrical imperfections

Figure 6(a) includes (i) the experimental equilibrium paths *P vs.* d_6 and *P vs.* d_7, where d_6 and d_7 are the measurements of transducers T6 and T7 (see Fig. 5(b) – inward displacements positive), and (ii) several numerical equilibrium paths involving the same displacements and concerning columns containing the IP1-IP7 initial geometrical imperfections – the table in this figure provides the corresponding failure loads (P_{Num}). As for Figure 6(b), it shows the column failure modes (deformed configurations very close to the peak load) observed experimentally and provided by the numerical simulation associated with the IP6 initial imperfections – the latter includes also the plastic strain distribution. On the other hand, Figures 7(a)-(g) and 8(a)-(g) make it possible to compare the deformed configurations at the onset of collapse of the columns containing IP1-IP7 initial geometrical imperfections: they concern, respectively, the (i) mid-span cross-section and (ii) top flange deformed configurations. The observation of all these results prompts the following comments:

(i) Naturally, the columns with "pure" initial imperfections (IP1-IP3) exhibit the three highest failure loads. Moreover, their collapse modes involve (i_1) combined local and distortional deformations (IP1 and IP2 – while the local deformations prevail in the former case, the opposite happens in the latter, which has a lower failure load), thus evidencing the presence of local-distortional interaction[4], and (i_2) exclusively global (flexural-

[4] Recall that column CP30 has (i) a critical local buckling load, (ii) distortional and flexural-torsional critical loads *12%* and *34%* higher, and (iii) the latter practically coincides with the squash load.

torsional) deformations (IP3 – apparently, and in spite of the content of footnote 4, the absence of local and/or distortional initial imperfections precludes the development of such deformations).

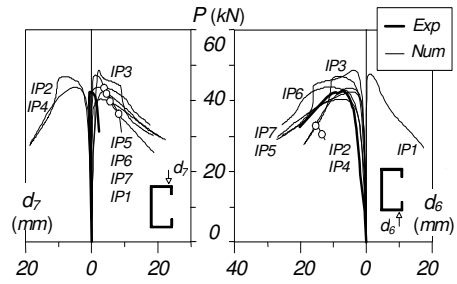

	Imperfection						
Mode	IP1	IP2	IP3	IP4	IP5	IP6	IP7
L	δ_0	–	–	δ_0	δ_0	–	δ_0
D	–	Δ_0	–	Δ_0	–	Δ_0	Δ_0
FT	–	–	β_0	–	β_0	β_0	β_0
P_{Num} (kN)	47.24	46.81	48.45	43.57	42.37	43.73	40.29
P_{Exp} (kN)	42.41						

(a)

(b)

Fig. 6: Numerical and experimental results concerning the CP30 specimen: (a) *P vs.* d_7 and *P vs.* d_6 equilibrium paths (IP1-IP7 imperfections), and (b) experimental and numerical (IP6 imperfections) failure mode configurations

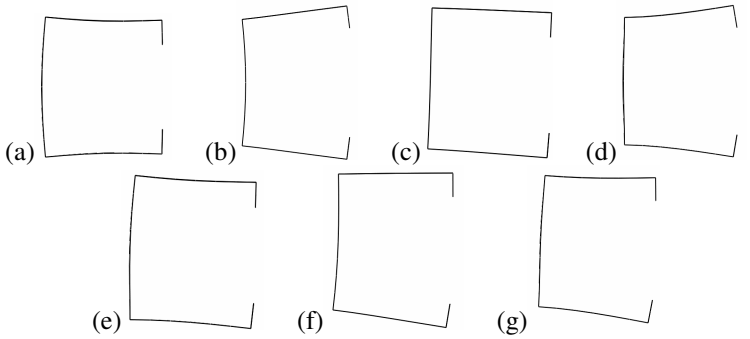

Fig. 7: Mid-span cross-section deformed configurations at collapse of CP30 columns containing (a) IP1, (b) IP2, (c) IP3, (d) IP4, (e) IP5, (f) IP6 and (g) IP7 imperfections

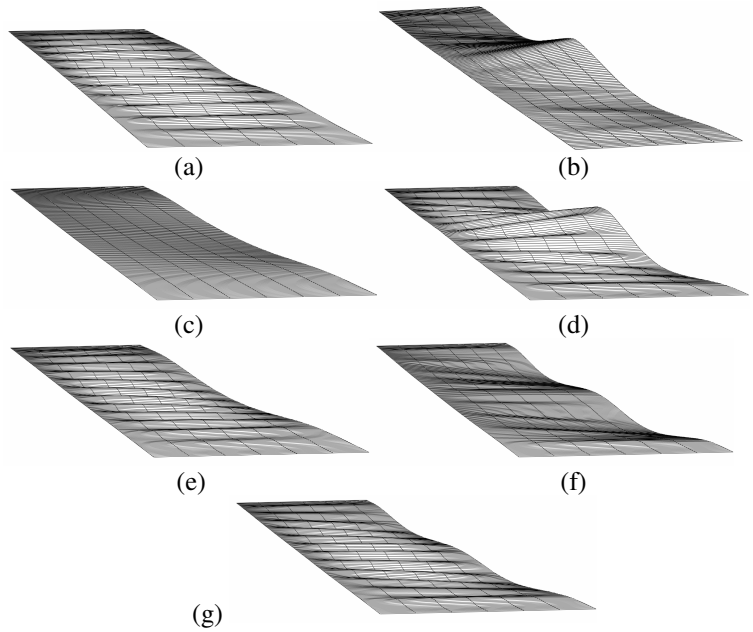

Fig. 8: Top flange deformed configurations at the onset of collapse of CP30 columns containing (a) IP1, (b) IP2, (c) IP3, (d) IP4, (e) IP5, (f) IP6 and (g) IP7 imperfections

(ii) Only the collapse mode of the column with IP3 initial imperfections does not exhibit local and distortional deformations. On the other hand, only the columns containing flexural-torsional initial imperfections (IP3, IP5-IP7) exhibit this type of deformations at failure.

(iii) Naturally, the local deformations are most perceptible in the columns having local initial imperfections (IP1, IP4, IP5, IP7). Such deformations are less visible in the columns with IP2 and IP6 initial imperfections, since the local deformations only appear due to the local-distortional interaction effects. Similarly, the distortional deformations are more (less) noticeable in the columns having IP2, IP4, IP6, IP7 (IP1, IP5) initial imperfections.

(iv) Since all the tested specimens (namely specimen CP30) failed in collapse modes exhibiting (iv_1) a combination of distortional and (predominant) flexural-torsional deformations, which evidences the occurrence of mild

distortional-global interaction, and (iv_2) the numerical failure load of the column containing the IP3 initial imperfection (the only one whose collapse mode does not exhibit local deformations) is about 15% higher than the test value (*48.45 kN* vs. *42.45 kN*), it seems fair to acknowledge that there is a discrepancy between the experimental and numerical test results. However, this discrepancy is consistent with the previous assertion that the test set-up that did not ensure fully fixed-ended support conditions. Indeed, even a small amount of major-axis flexural rotation will certainly lower the critical flexural-torsional and distortional buckling loads (mostly the former), while keeping their local counterpart practically unchanged (due to the very large number of half-waves, the influence of the end support conditions is marginal), thus providing a logical explanation for the failure mode observed experimentally and the corresponding failure load.

(v) In spite of what was mentioned in the previous item, it is fair to argue that there is a fairly good correlation between the experimental failure mode and its numerical counterpart obtained for the column containing the IP6 initial imperfection – note, however, that the latter exhibits a small amount of local deformation, reported to be completely absent in the former.

(vi) An more thorough numerical investigation is planned for the near future, in order to acquire in-depth knowledge concerning the (vi_1) column imperfection sensitivity (taking into account also the initial imperfection longitudinal profile, which was measured in the tested specimens) and (vi_2) influence of not fully restraining the end section flexural rotations.

DSM Design Considerations

The currently available and codified DSM design curves can be found in Schafer's state-of-the-art report (2008) and provide column nominal strengths against local, distortional, global and local-global interactive failures (f_{NL}, f_{ND}, f_{NE} and f_{NLE}) – in the last case, f_y is replaced by f_{NE} in the f_{NL} expressions. However, no similarly well-established and consensual strength curves are yet available for the design against interactive failures involving distortional buckling. In the particular case of local-distortional interactive failures, a procedure akin to the one adopted to handle columns failing in local-global interactive modes led to the development and proposal of design curves to estimate the ultimate strength of columns experiencing L-D interaction, based on the replacement of f_y by f_{ND} in the f_{NL} equations (f_{NLD} approach) (Schafer

2002, Yap & Hancock 2004) – this procedure was subsequently modified and successfully adopted to estimate failure loads of (i) plain, web-stiffened and web/flange-stiffened lipped channel columns undergoing L-D interaction (Kwon *et al.* 2009) and (ii) lipped channel columns (Silvestre *et al.* 2012) exhibiting strong L-D interaction[5]. Similarly, it was argued by Yap & Hancock (2011) that safe and accurate failure load estimates against distortional-global interactive failures can be obtained by replacing f_y with f_{NE} in the f_{ND} equations, thus leading to the f_{NDE} approach. Carrying this reasoning one step further, those authors contended that it may be possible to predict the ultimate strength of cold-formed steel columns experiencing triple (L-D-G) interaction by means of a f_{NLDE} approach, obtained from the f_{NL} expression by replacing f_y with f_{NDE} – note that this approach was successfully employed to estimate the failure loads of web-stiffened and web/flange-stiffened lipped channel columns (Yap & Hancock 2011)[6]. The column nominal ultimate strength predictions against interactive failures involving global deformations are then given by:

$$f_{NLE} = \begin{cases} f_{NE} & if \quad \lambda_{LE} \le 0.776 \\ f_{NE}\left(\frac{f_{CRL}}{f_{NE}}\right)^{0.4}\left[1-0.15\left(\frac{f_{CRL}}{f_{NE}}\right)^{0.4}\right] & if \quad \lambda_{LE} > 0.776 \end{cases} \quad , (1)$$

$$f_{NDE} = \begin{cases} f_{NE} & if \quad \lambda_{DE} \le 0.561 \\ f_{NE}\left(\frac{f_{CRD}}{f_{NE}}\right)^{0.6}\left[1-0.25\left(\frac{f_{CRD}}{f_{NE}}\right)^{0.6}\right] & if \quad \lambda_{DE} > 0.561 \end{cases} \quad , (2)$$

$$f_{NLDE} = \begin{cases} f_{NDE} & if \quad \lambda_{LDE} \le 0.776 \\ f_{NDE}\left(\frac{f_{CRL}}{f_{NDE}}\right)^{0.4}\left[1-0.15\left(\frac{f_{CRL}}{f_{NDE}}\right)^{0.4}\right] & if \quad \lambda_{LDE} > 0.776 \end{cases} \quad , (3)$$

where $\lambda_{LE}=(f_{NE}/f_{CRL})^{0.5}$, $\lambda_{DE}=(f_{NE}/f_{CRD})^{0.5}$ and $\lambda_{LDE}=(f_{NDE}/f_{CRL})^{0.5}$.

Figure 9(a) shows four DSM strength curves (E, LE, DE and LDE), plotted against the global slenderness λ_E (under the assumption that $\lambda_E \approx \lambda_D \approx \lambda_L$, which is not exactly the case), together with the fixed-ended lipped channel column

[5] Later, Dinis & Camotim (2014) extended these findings to hat, zed and rack-section columns.

[6] This DSM approach involved the modification of the existing local strength/design curve (f_{NLo}).

experimental f_U/f_y values (f_y is the measured yield stress) concerning the *17* specimens dealt with in this work (CP2-CP32-1 columns). Moreover, Figure 9(b) also displays results of fixed-ended lipped channel column experiencing different levels of L-D-G interaction: (i) *134* numerical f_{Num}/f_y values obtained by Dinis *et al.* (2012), and (ii) *33* experimental f_{Exp}/f_y values concerning (ii_1) *16* tests reported by Young *et al.* (2013) and Dinis *et al.* (2014) (white circles), (ii_2) *12* tests reported by Santos *et al.* (2012) (grey circles) and (ii_3) *5* tests reported by Kwon *et al.* (2009) (black circles). It is worth noting that (i) the experimental and numerical failure loads reported by Santos *et al.* (2012) and Dinis *et al.* (2012) concern columns with close local, distortional and global critical buckling loads ($1.00 \leq P_{cr.max}/P_{cr.min} \leq 1.10$)[7] and $P_y/P_{cr.max}$ values in the *1.19-2.16* (experimental) and *0.53-6.24* (numerical) ranges, (ii) the tests reported by Santos *et al.* (2012) exhibited mostly D-G interactive failures, with no local deformations visible, (iii) the tests reported by Young *et al.* (2013) dealt with columns exhibiting $1.11 \leq P_{cr.max}/P_{cr.min} \leq 1.39$ and $P_y/P_{cr.max}$ values in the *1.62-3.61* range and (iv) out of the tests reported by Kwon *et al.* (2009) only those concerning plain lipped channel columns with $1.17 \leq P_{cr.max}/P_{cr.min} \leq 1.56$ and $P_y/P_{cr.max}$ values in the *1.27-2.27* range were considered (*i.e.*, only the ones with ranges similar to those characterizing the CP2-CP32 column specimens dealt with in this work: $P_{cr.max}/P_{cr.min}$ and $P_y/P_{cr.max}$ values in the *1.08-1.44* and *1.01-1.82* ranges, respectively). Finally, Figures 10(a)-(c) plot the ratios f_U/f_{NLE}, f_U/f_{NDE}, f_U/f_{NLDE}, concerning all failure loads, against λ_E – the corresponding

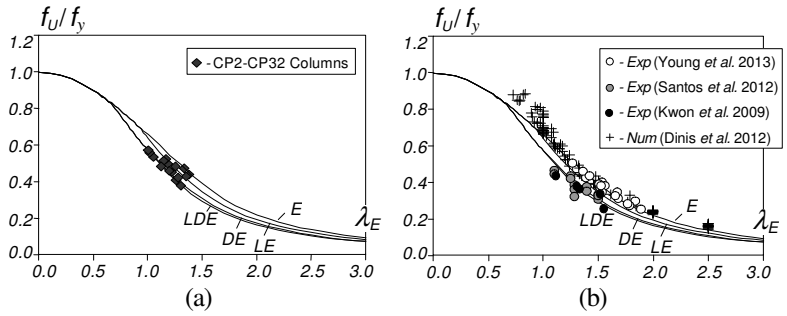

Fig.9: Plots of f_U/f_y against the global slenderness λ_E for (a) the CP2-CP32 columns and (b) the remaining available experimental and numerical column failure loads

[7] Assuming fixed-ended support conditions, probably not ensured by the experimental test set-up.

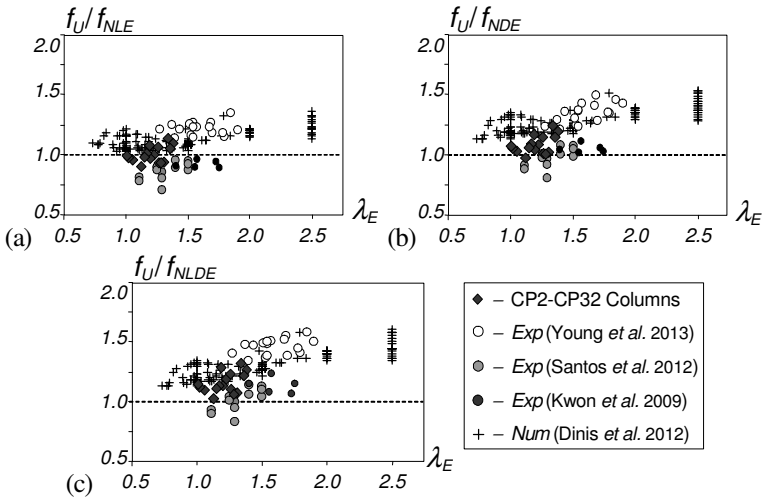

Fig. 10: Plots of (a) f_U/f_{NLE}, (b) f_U/f_{NDE} and (c) f_U/f_{NLDE} against the global slenderness λ_E

Table 3: Means and standard deviations of the failure-to-predicted ultimate strength ratios

			f_U/f_{NLE}	f_U/f_{NDE}	f_U/f_{NLDE}
Numerical		*Mean*	1.13	1.28	1.31
Dinis *et al.* (2012)		*S. Deviation*	0.08	0.10	0.11
Experimental	CP2-CP32 Columns	*Mean*	1.00	1.09	1.16
		S. Deviation	0.06	0.07	0.08
	Young *et al.* (2013)	*Mean*	1.22	1.34	1.46
		S. Deviation	0.05	0.07	0.07
	Santos *et al.* (2012)	*Mean*	0.86	0.97	1.01
		S. Deviation	0.07	0.08	0.09
	Kwon *et al.* (2009)	*Mean*	0.92	1.05	1.14
		S. Deviation	0.03	0.04	0.07

average and standard deviation values are given in Table 3. The observation of these results makes it possible to conclude that:

(i) The f_{NE} curve lies above a large fraction of the plotted experimental and numerical column failure loads. Moreover, it is worth noting that all the experimental values reported by Santos *et al.* (2012) fall well below all the remaining ones (including those concerning the CP2-CP32 columns) – even if there is no definitive explanation for this fact, it seems that it is due to the inability of the test set-up to ensure fixed-ended support conditions[8].

(ii) The f_{NLE} estimates of the (ii_1) experimental failure loads concerning the CP2-CP32 tested specimens and the tests reported by Kown *et al.* (2009) and Young *et al.* (2013), and (ii_2) numerical ultimate strengths obtained by Dinis *et al.* (2012) exhibit a relatively similar quality, even if the first two sets of predictions are on the unsafe side[9] – the corresponding averages and standard deviations read *1.00*/*0.06*, *0.92*/*0.03*, *1.22*/*0.05* and *1.13*/*0.08*, respectively. This means that the current DSM local-global interactive design curve predicts the above failure loads reasonably well.

(iii) Obviously, the f_{NDE} and f_{NLDE} estimates of the failure loads mentioned in the previous item are lower than their f_{NLE} counterparts, which means that noticeably higher (but also more scattered) underestimations are obtained – for instance, the averages and standard deviations of the f_{NDE} and f_{NLDE} estimates concerning the CP2-CP32 columns increase to *1.09*/*0.07* and *1.16*/*0.08*, respectively.

(iv) Although the f_{NLDE} values provide safe predictions for almost all the available (experimental and numerical) failure loads concerning lipped channel columns affected by L-D-G interaction (including several quite low ones reported by Santos *et al.* 2012), the underestimations are excessive in a fairly large number of cases. Therefore, the careful planning and performance of further experimental tests and numerical simulations, involving columns with well controlled $P_{cr.max}/P_{cr.min}$ and $P_y/P_{cr.max}$ values, is required before a satisfactory DSM design approach can be reached.

---

[8] As far as the end support conditions are concerned, there was a clear improvement between the first and second test programs carried out at the Federal University of Rio de Janeiro, even if it seems that the fully fixed-ended support conditions have not yet been achieved.

[9] It should be pointed out that the test set-up employed by Kwon *et al.* (2009) involved the use of a capping system made of unsaturated polyester resin. Very recently, in the context of an investigation on web-stiffened columns, Martins *et al.* (2014) cast some doubts concerning the full fixity of the column end sections – the current overestimations seem to confirm their assertion.

Conclusion

This paper presented experimental, numerical and design results concerning an ongoing investigation on the post-buckling and ultimate strength behavior of cold-formed steel fixed-ended lipped channel columns affected by local-distortional-global interaction. After briefly addressing the column geometry selection, the paper focused on the experimental test program, carried out at the Federal University of Rio de Janeiro, namely on its output: steel material properties, initial geometrical imperfections, post-buckling equilibrium paths and ultimate loads. Then, the paper addressed the numerical (ABAQUS shell finite element analysis) simulation of one tested specimen – the agreement with the experimental values was found to be reasonable, even if a few discrepancies detected remain to be fully explained (probably, the test set-up did not ensure fully fixed-ended support conditions). The paper closed with some remarks on the DSM design of columns affected by L-D-G interaction. Several DSM-based design curves, some of them accounting for mode interaction phenomena, were compared with numerical and experimental failure loads available in the literature, including those dealt with in this paper. It was found that the current DSM design curve provides acceptable failure load predictions against local-global interactive failures – however, further experimental and numerical research, involving columns with various $P_{cr.max}/P_{cr.min}$ and $P_y/P_{cr.max}$ values, is required before a satisfactory DSM-based design approach can be reached.

References

Bebiano R, Pina P, Silvestre N, Camotim D (2008). *GBTUL 1.0β – Buckling and Vibration Analysis of Thin-Walled Members*, DECivil, IST, Technical University of Lisbon. (freely available at *http://www.civil.ist.utl.pt/gbt*)

Camotim D, Dinis PB (2013). Distortional-global interaction in lipped channel columns, *ICE-Structures and Buildings*, **166**(8), 381-391.

Dinis PB, Camotim D (2011). Local/distortional/global mode interaction in simply supported cold-formed steel lipped channel columns, *International Journal of Structural Stability and Dynamics*, **11**(5), 877-902.

Dinis PB, Camotim D (2014). Cold-formed steel columns undergoing local-distortional coupling: behaviour and direct strength prediction against interactive failure, *Computers & Structures*, accepted for publication.

Dinis PB, Camotim D, Batista E, Santos E (2011). Local/distortional/global mode coupling in fixed lipped channel columns: behaviour and strength, *Advanced Steel Construction*, **7**(4), 113-130.

Dinis PB, Batista EM, Camotim D, Santos ES (2012). Local-distortional-global interaction in lipped channel columns: Experimental results, numerical simulations and design considerations, *Thin-Walled Structures*, **61**(December), 2-13.

Dinis PB, Young B, Camotim D (2014). L-D-G interaction in CFS lipped channel columns: experimental results, numerical simulations and design considerations, *Proceedings of 7th European Conference on Steel and Composite Structures* (EUROSTEEL 2014 – Naples, 10-12/9), in press.

Dubina D, Ungureanu V, Crisan A (2013). Experimental evidence of erosion of critical load in interactive buckling, *Journal of Structural Engineering* (ASCE), **139**(5), 705-716.

Kwon YB, Kim BS, Hancock GJ (2009). Compression tests of high strength cold-formed steel channels with buckling interaction, *Journal of Constructional Steel Research*, **65**(2), 278-89.

Martins AD, Dinis PB, Camotim D, Providência P (2014). On the influence of local-distortional interaction in the behavior and design of cold-formed steel web-stiffened lipped channel columns, *Proceedings of 22nd International Specialty Conference on Cold-Formed Steel Structures* (St. Louis, 5-6/11), in press.

Rossi B, Jaspart JP, Rasmussen KJR (2010). Combined distortional and overall flexural-torsional buckling of cold-formed stainless steel sections: experimental investigations, *Journal of Structural Engineering* (ASCE), **136**(4), 354-360.

Santos ES, Batista EM, Camotim D (2012). Experimental investigation concerning lipped channel columns undergoing local-distortional-global buckling mode interaction, *Thin-Walled Structures*, **54**, 19-34.

Santos ES, Batista EM, Camotim D (2014). Cold-formed steel columns under L-D-G interaction: experimental investigation, *Proceedings of 7th European Conference on Steel and Composite Structures* (EUROSTEEL 2014 – Naples, 10-12/9), in press.

Schafer BW (2002). Local, distortional and Euler buckling in thin-walled columns, *Journal of Structural Engineering* (ASCE), **128**(3), 289-299.

Schafer BW (2008). Review: the direct strength method of cold-formed steel member design, *Journal of Constructional Steel Research*, **64**(7-8), 766-778.

Silvestre N, Camotim D, Dinis PB (2012). Post-buckling behaviour and direct strength design of lipped channel columns experiencing local-distortional interaction, *Journal of Constructional Steel Research*, **73**(June), 12-30.

Yap DCY, Hancock GJ (2004). Compression tests of high strength steel columns with interaction between local and distortional buckling", *Journal of Structural Engineering* (ASCE), **130**(12), 1954-1963.

Yap DCY, Hancock GJ (2011). Experimental study of high strength cold-formed stiffened web steel sections, *Journal of Structural Engineering* (ASCE), **137**(2), 162-172.

Young B, Camotim D, Dinis PB (2013). Tests of cold-formed steel lipped channel columns undergoing local-distortional-global interaction, *Research and Applications in Structural Engineering, Mechanics and Computation* (SEMC 2013 – Cape Town, 2-4/9), A. Zingoni (ed.), Taylor & Francis (London), 387-388. (full paper in CD-ROM Proceedings – 1071-1076)